

## Design of a Novel Miniaturized Wide Stopband Filtering Coupler

Xiaming Mo<sup>1</sup>, Yongkang Yuan<sup>1</sup>, Minquan Li<sup>1, \*</sup>, Pingjuan Zhang<sup>2</sup>,  
Yajing Yan<sup>1</sup>, Guangxiu Zhao<sup>1</sup>, and Ziyun Tu<sup>1</sup>

**Abstract**—This paper designs a miniaturized, wide stopband microstrip filtering coupler based on coupled resonators. Firstly, a short-stub loaded uniform-impedance resonator (SSLUIR) is proposed, and the size of the SSLUIR is reduced by adjusting the impedance ratio of the stubs and bending them. Then, the resonance performance of SSLUIR during electrical and magnetic coupling is studied. By adjusting the electrical length of the short stubs, higher harmonics are suppressed, and the upper stopband is widened. Finally, a 3 dB 180° microstrip filtering coupler is designed based on SSLUIRs. The measurement results show that the center frequency of the filtering coupler is 2.43 GHz, with a relative bandwidth of 6.6%. It can suppress harmonics within the  $8.2f_0$  range by more than 18 dB and has a size of  $0.23\lambda_g \times 0.33\lambda_g$ . The correctness of the design method for miniaturized and wide stopband filtering coupler has been verified.

### 1. INTRODUCTION

As the size of mobile terminals continues to decrease, the requirements for miniaturization and integration of circuits and devices are also constantly increasing [1–3]. As a key component of wireless communication systems, the research on filtering couplers is of great significance. In traditional wireless communication systems, filters and couplers are cascaded together, which not only leads to larger circuit sizes but also leads to additional losses due to stage mismatch. To solve this problem, one design solution is to integrate the filter and coupler for design.

At present, there are two main directions for the design of microstrip filtering couplers: the first is the design of harmonic suppression couplers based on transmission line resonators [4–9], and the second is the design of filtering couplers based on coupled resonators with bandpass response [10–13]. The design method of harmonic suppression couplers based on transmission line resonators usually uses transmission lines with frequency selection characteristics to replace the traditional  $1/4$  wavelength transmission lines of couplers. The design process is simple, but lacks bandpass response and is large in size. In [4], a branch-line hybrid (BH) topology is suggested, and a compact equivalent circuit of a transmission-line is suggested for harmonic suppression BH which can be applied to all possible power-division ratios. [6] achieved a coupled line forward directional coupler with inherent harmonics suppression at  $2f_0$  by using the inductor loaded coupled line and inserting the open-circuited stubs. In [7], a coupler with high harmonic suppression function was designed by loading stepped impedance stubs on the transmission line. [8] proposes branch line couplers with compact size and harmonic suppression based on non-periodic reactively loaded artificial lines. The reactive loading elements of the lines provide transmission zeros, which suppress the harmonic content of the device efficiently. In [10], a filtering coupler that can achieve power distribution, phase shift, and bandpass response was designed by combining four half wavelength uniform impedance resonators. A wide stopband filtering

---

Received 2 July 2023, Accepted 13 September 2023, Scheduled 26 September 2023

\* Corresponding author: Minquan Li (AHU411MHz@hotmail.com).

<sup>1</sup> Key Lab of Ministry of Education of Intelligent Computing & Signal Processing, Anhui University, Hefei 230601, China. <sup>2</sup> Anhui Science and Technology University, Bengbu 233100, China.

coupler composed of coupling lines and stepped impedance units is proposed in [11], which can suppress harmonics within the  $5.24f_0$  range by more than 10 dB. [12] designed a novel wideband coupled-line filtering coupler for arbitrary high power-division ratios, a modified stepped impedance resonator (SIR) with a self-coupled section is proposed in [13], which is employed to design a class of compact dual-band bandpass filters (BPFs) with wide controllable range of frequency ratio. The filter based on self-coupled resonator has good performances of no frequency dispersion in wideband and compact size, but does not have harmonic suppression characteristics.

This paper integrates the design of filters and couplers, and designs a miniaturized, wide stopband filtering coupler. Firstly, a short-stub loaded uniform-impedance resonator was designed, and its resonant characteristics were analyzed using the  $ABCD$  matrix and admittance  $Y$  parameters. By adjusting the impedance ratio of the stubs and bending them, the size of the SSLUIR was effectively reduced. Then, the resonance performance of SSLUIR during electrical and magnetic coupling was studied, by adjusting the electrical length of the short stub, introducing a transmission zero point, suppressing high-order harmonics, and achieving a wide stopband. Finally, a 3 dB  $180^\circ$  microstrip filtering coupler is designed based on SSLUIRs by using the analysis method of external quality factor and coupling coefficient. According to the results, the center frequency of the filtering coupler is 2.43 GHz, with a relative bandwidth of 6.6%. The minimum insertion loss is 3.9 dB, which includes a filtering loss of 0.9 dB and a power distribution of 3 dB. The isolation degree is greater than 20 dB, and the harmonic suppression within the  $8.2f_0$  range is more than 18 dB. The phase imbalance in the passband does not exceed  $9^\circ$ ; the amplitude imbalance does not exceed 1.2 dB; and the size of the filtering coupler is  $0.23\lambda_g \times 0.33\lambda_g$ . The measurement results indicate that the filtering coupler has excellent performance, miniaturization, and wide stop-band characteristics.

## 2. RESONANCE CHARACTERISTICS OF SSLUIR

This paper proposes an SSLUIR to design a filtering coupler, as shown in Fig. 1.  $Y_1$  and  $Y_2$  represent the characteristic admittance of the uniform impedance transmission line and the short stub transmission

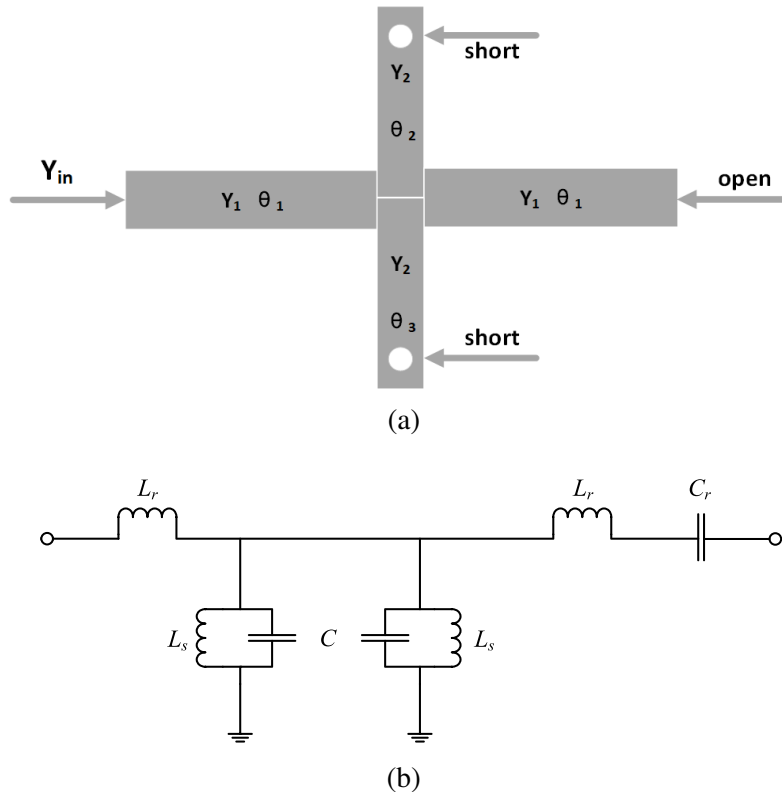


**Figure 1.** (a) Short-stub loaded uniform-impedance resonator. (b) Equivalent circuit.

line, while  $\theta_1, \theta_2, \theta_3$  represent electrical length.

Using the  $ABCD$  matrix for analysis, the input admittance values are obtained through network transformation. For convenience, in the following analysis, only the lossless case is considered. According to the  $ABCD$  matrix theory of transmission lines, the  $ABCD$  matrix of each transmission line can be obtained. The  $ABCD$  matrices of uniform impedance transmission lines and short stub transmission lines are represented as  $M_{\text{line1}}, M_{\text{stub1}},$  and  $M_{\text{stub2}},$  respectively:

$$M_{\text{line1}} = \begin{bmatrix} \cos \theta_1 & jZ_1 \sin \theta_1 \\ jY_1 \sin \theta_1 & \cos \theta_1 \end{bmatrix} \quad (1)$$

$$M_{\text{stub1}} = \begin{bmatrix} 1 & 0 \\ -jY_2 \cot \theta_2 & 1 \end{bmatrix} \quad (2)$$

$$M_{\text{stub2}} = \begin{bmatrix} 1 & 0 \\ -jY_2 \cot \theta_3 & 1 \end{bmatrix} \quad (3)$$

The  $ABCD$  matrix of SSLUIR can be expressed as:

$$\begin{aligned} & \begin{bmatrix} A & B \\ C & D \end{bmatrix} \\ &= M_{\text{line1}} \times M_{\text{stub1}} \times M_{\text{stub2}} \times M_{\text{line1}} \\ &= \begin{bmatrix} \cos 2\theta_1 + \frac{Z_1 \sin 2\theta_1 (Y_2 \cot \theta_2 + Y_2 \cot \theta_3)}{2} & jZ_1 \sin 2\theta_1 + jZ_1^2 \sin^2 \theta_1 (Y_2 \cot \theta_2 + Y_2 \cot \theta_3) \\ jY_1 \sin 2\theta_1 - j \cos^2 \theta_1 (Y_2 \cot \theta_2 + Y_2 \cot \theta_3) & \cos 2\theta_1 + \frac{Z_1 \sin 2\theta_1 (Y_2 \cot \theta_2 + Y_2 \cot \theta_3)}{2} \end{bmatrix} \end{aligned} \quad (4)$$

By converting the  $ABCD$  matrix to the admittance parameter, it can be concluded that:

$$\begin{aligned} Y_{in} &= \frac{C}{A} = \frac{jY_1 \sin 2\theta_1 - j \cos^2 \theta_1 (Y_2 \cot \theta_2 + Y_2 \cot \theta_3)}{\cos 2\theta_1 + \frac{Z_1 \sin 2\theta_1 (Y_2 \cot \theta_2 + Y_2 \cot \theta_3)}{2}} \\ &= \frac{j2Y_1^2 - jY_1 \cot \theta_1 (Y_2 \cot \theta_2 + Y_2 \cot \theta_3)}{2Y_1 \cot 2\theta_1 + Y_2 \cot \theta_2 + Y_2 \cot \theta_3} \end{aligned} \quad (5)$$

For the convenience of analysis, assuming  $\theta_1 = \theta_2 = \theta_3 = \theta,$  (5) is transformed into:

$$Y_{in} = \frac{jY_1^2 - jY_1 Y_2 \cot^2 \theta}{Y_1 \cot 2\theta + Y_2 \cot \theta} \quad (6)$$

If  $Y_{in} = 0,$  the resonance conditions can be obtained as follows:

$$\theta = \arccot \sqrt{\frac{Y_1}{Y_2}} \quad (7)$$

When  $Y_1 = Y_2$  and  $\theta = 45^\circ,$  the electrical length of the uniform impedance transmission line is one quarter of the working wavelength. By setting the impedance ratio  $K = Y_1/Y_2 = Z_2/Z_1,$  between the short stub and the uniform impedance transmission line, and normalizing the electrical length of the transmission line with  $\theta = 45^\circ,$  a function image between the electrical length  $\theta$  and the impedance ratio  $K$  can be constructed, as shown in Fig. 2.

### 3. DESIGN AND ANALYSIS

#### 3.1. Magnetic Coupling Analysis

The magnetic coupling between resonators is achieved through short-circuit coupling lines, as shown in Fig. 3(a). In order to reduce the circuit area, the loaded open and short stubs are bent. According to transmission line theory, by adjusting the length of the circuit, a phase difference of  $-90^\circ$  can be obtained. Fig. 3(b) shows the simulation results of the  $S$ -parameters of the resonator connected by magnetic coupling. It can be seen that the center frequency of the passband is 2.4 GHz, and the width of the upper stopband exceeds  $8f_0,$  indicating that the circuit has a wide stopband characteristic.

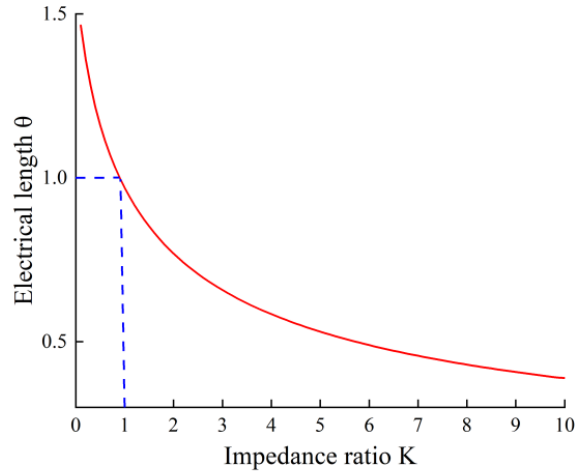


**Figure 2.** The variation curve of electrical length  $\theta$  with impedance ratio  $K$ .

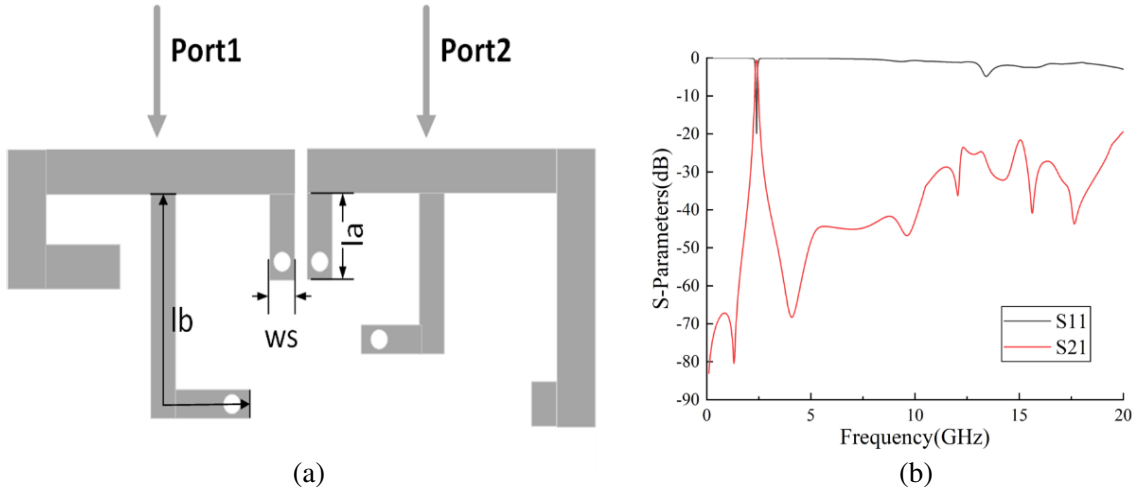


**Figure 3.** (a) Magnetic coupled resonant circuit. (b)  $S$ -parameter simulation result.

Keeping the other parameters of the resonant circuit unchanged and changing the length of the short stub  $lb$ , it can be seen from Fig. 4(a) that when  $lb$  changes from 12.1 mm to 11.1 mm, higher-order harmonics appear in the upper stopband of the resonant circuit. This is because the length of the short stub is no longer equal to the quarter wavelength corresponding to the higher-order harmonics, so it is unable to suppress higher-order harmonics, and parasitic passbands appear. Keeping the other parameters of the resonant circuit unchanged and changing the width of the short stub  $ws$ , it can be seen from Fig. 4(b) that as the stub width increases, the center frequency of the resonant circuit moves towards the high-frequency direction. This is due to the decrease in impedance ratio between the short stub and the open stub.

### 3.2. Electrical Coupling Analysis

The electrical coupling between resonators is achieved through open circuit coupling lines, as shown in Fig. 5(a). In order to reduce the circuit size, the loaded open and short stubs are bent. According to transmission line theory, by adjusting the length of the circuit, a  $90^\circ$  phase difference can be achieved. Fig. 5(b) shows the simulation results of the  $S$ -parameters of the resonator connected by electrical coupling. It can be seen that the center frequency of the passband is 2.4 GHz, and the width of the

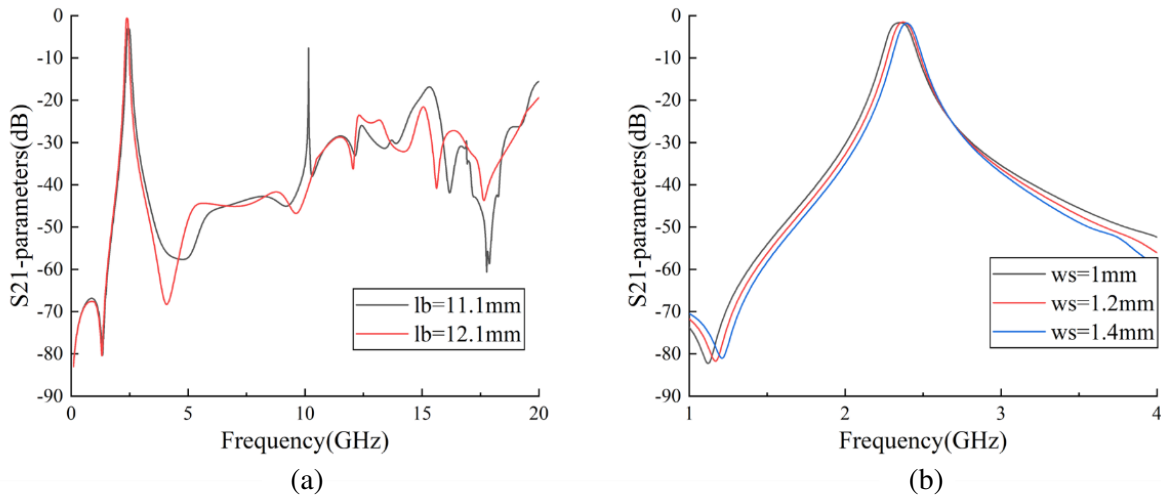


Figure 4. (a) The influence of  $lb$  on  $S_{21}$ . (b) The influence of  $ws$  on  $S_{21}$ .

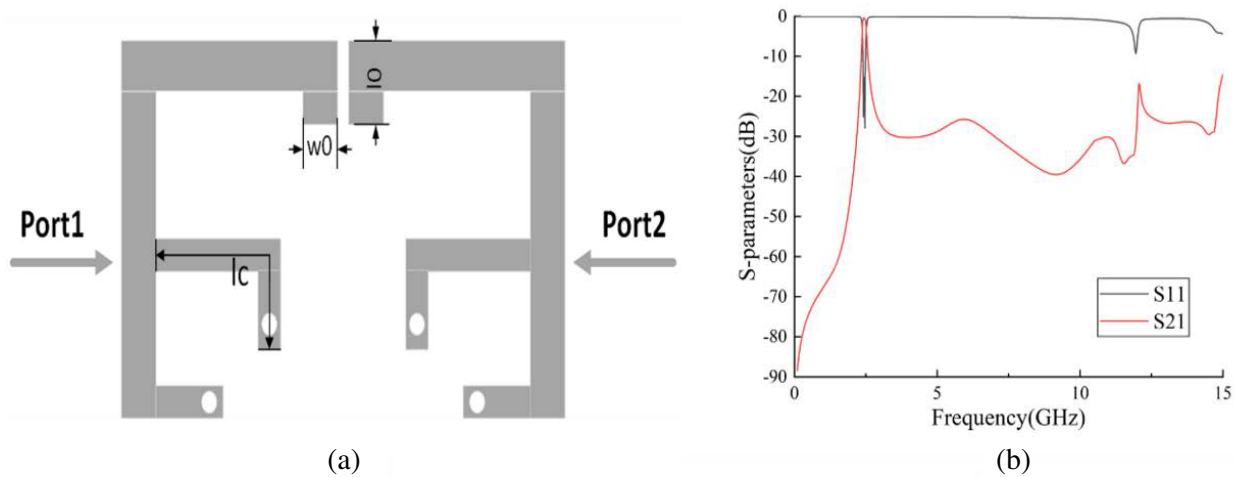


Figure 5. (a) Electrically coupled resonant circuit. (b)  $S$ -parameter simulation result.

upper stopband exceeds  $6f_0$ , indicating that the circuit has a wide stopband characteristic.

Keeping the other parameters of the resonant circuit unchanged and changing the length of the short stub  $lc$ , it can be seen from Fig. 6(a) that when  $lc$  changes from 7.8 mm to 8.8 mm, higher-order harmonics appear in the upper stopband of the resonant circuit, causing the upper stopband to become narrow. Keeping the other parameters of the resonant circuit unchanged and changing the length of the open stub  $l_0$ , it can be seen from Fig. 6(b) that as the length of the stub increases, the phase of the resonant circuit passband gradually decreases. Therefore, the required phase can be obtained by selecting an appropriate electrical length.

### 3.3. External Quality Factor Analysis

This article designs a new type of microstrip  $180^\circ$  filtering coupler, which has a center frequency of 2.4 GHz, a coupling ratio of 3 dB, a relative bandwidth of 4%, a passband ripple of 0.1 dB, and a corresponding return loss of 16.4 dB. According to the indicators, the parameters of the low-pass prototype filter are:  $g_1 = 0.8431$ ,  $g_2 = 0.6220$ , and  $g_3 = 1.3554$ . After the design index of filtering coupler is determined, the corresponding external quality factor of input and output can be obtained

as  $Q_{e1} = Q_{e2} = 21.1$ . The HFSS electromagnetic simulation software is used to extract the relationship between the gap between the input and output ports and the resonator and the external quality factor. Fig. 7(a) shows the structure corresponding to extracting the external quality factor, and Fig. 7(b)

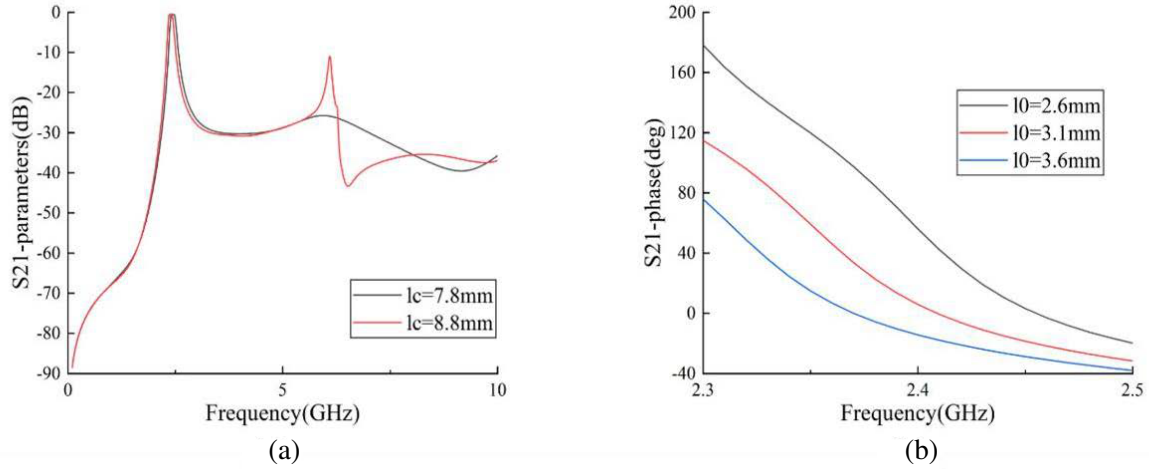


Figure 6. (a) The influence of  $l_c$  on  $S_{21}$ . (b) The influence of  $l_0$  on  $S_{21}$ .

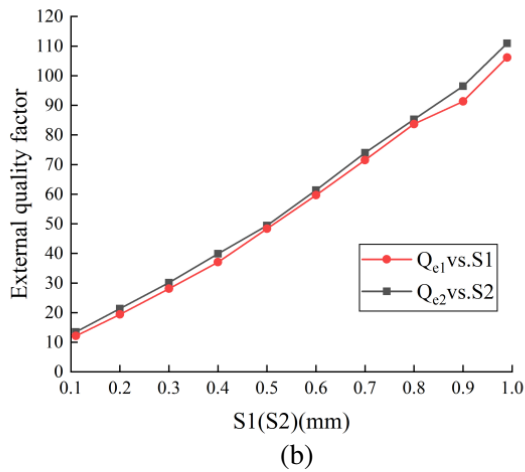
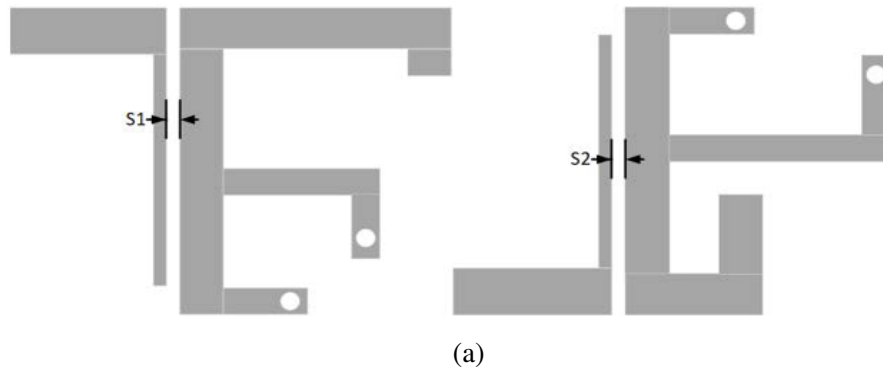
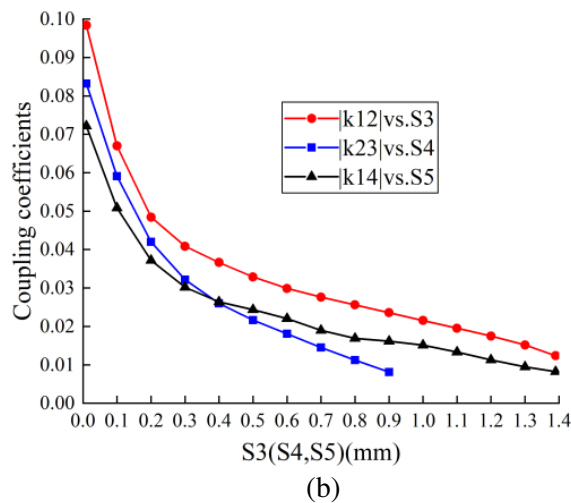
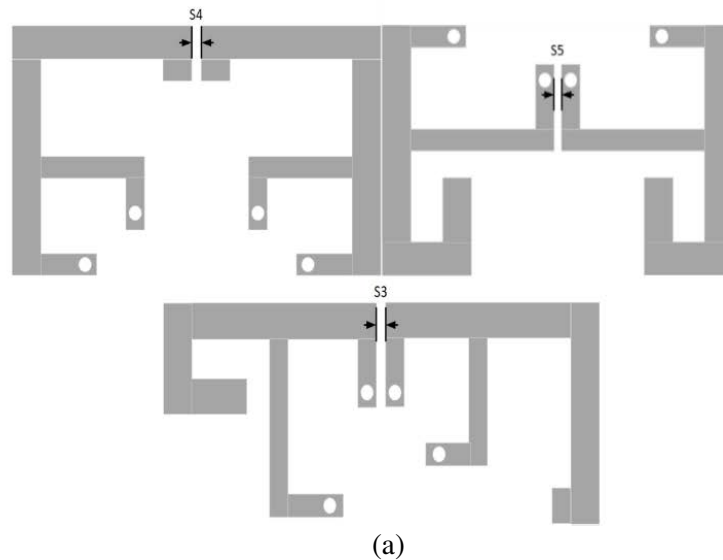


Figure 7. (a) Structure of extracting external quality factor. (b) Relationship between the gap between the port and the resonator and the external quality factor.

shows the relationship between the distance ( $S1$  and  $S2$ ) between the input and output ports and the resonator and the external quality factor. Compare the extracted  $Q_e$  values with the theoretical  $Q_e$  values to select the most suitable coupling gap. It can be seen from Fig. 7 that the initial value of coupling gap corresponding to the theoretical external quality factor  $S1 = S2 = 0.2$  mm.

### 3.4. Coupling Coefficient Analysis

After determining the design indicators of the filtering coupler, the coupling coefficient between adjacent resonators can be calculated as  $k_{12} = -k_{23} = k_{34} = k_{14} = 0.033$ . HFSS is used to extract the relationship between the gap and coupling coefficient between adjacent resonators. The structure corresponding to the extraction of coupling coefficients is shown in Fig. 8(a), and the relationship between the coupling gaps ( $S3, S4$ , and  $S5$ ) between resonators and the coupling coefficients is shown in Fig. 8(b). The extracted  $k$  values are compared with the theoretical  $k$  ones to select the most suitable coupling gap. From the figure, it can be seen that the initial coupling gap values  $S3 = 0.5$  mm and  $S4 = S5 = 0.3$  mm corresponding to the required coupling coefficient.



**Figure 8.** (a) Structure for extracting coupling coefficients. (b) The relationship between the gap between adjacent resonators and the coupling coefficient.

### 4. MEASUREMENT AND ANALYSIS

In order to verify the above method, a  $180^\circ$  coupler with bandpass response of microstrip structure is designed and fabricated on a Rogers4730 dielectric substrate with dielectric constant  $\epsilon_r = 3$ , loss tangent  $\delta = 0.0023$ , and thickness  $h = 1$  mm. The structure layout is shown in Fig. 9. HFSS software is used to model, simulate, and optimize the structure of the filtering coupler, and finally determine the main parameters as shown in Table 1. The size of the filtering coupler is  $18\text{ mm} \times 26\text{ mm}$  ( $0.23\lambda_g \times 0.33\lambda_g$ ). The optimized optimal structure is processed and tested, and the processed filtering coupler is shown in Fig. 10.

When port 1 is the input port, the comparison between the measured and simulated results of the  $S$ -parameter is shown in Fig. 11. For ease of observation, the broadband and narrowband results are

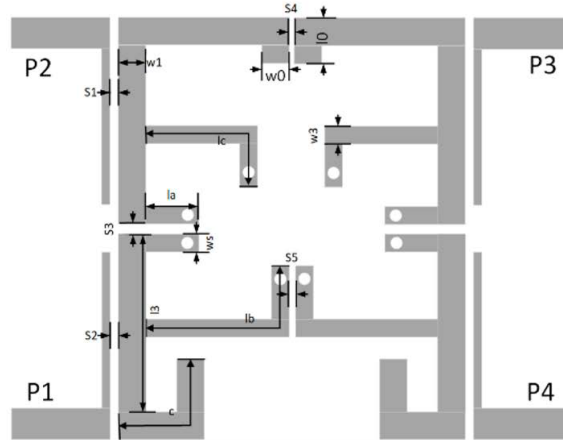


Figure 9. Filtering coupler layout.

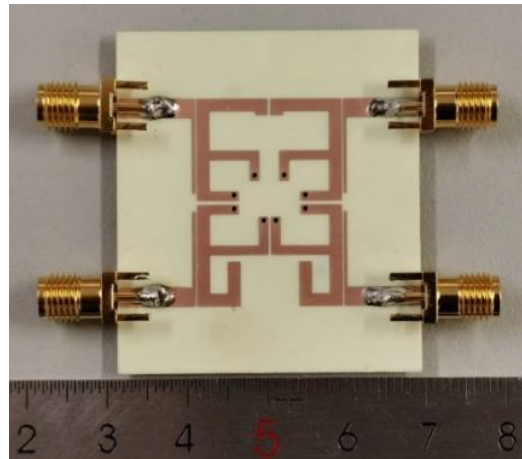
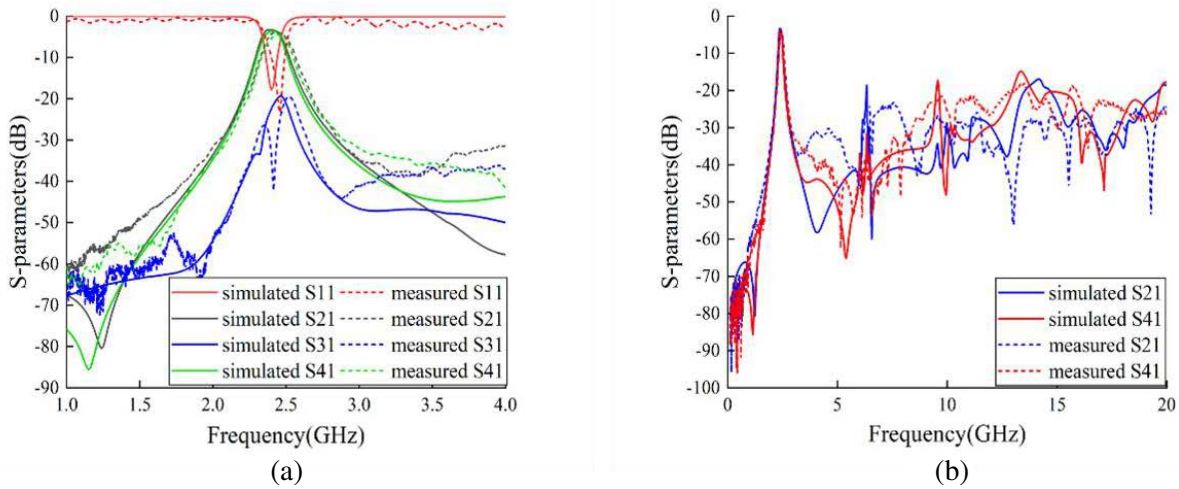


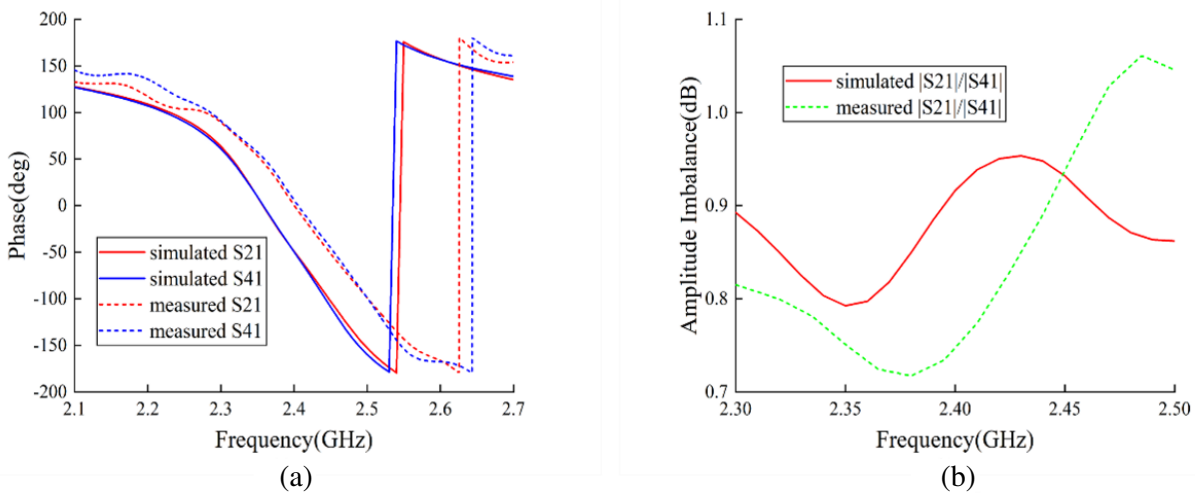
Figure 10. Physical image of filtering coupler.

Table 1. Main size parameters of filtering coupler (unit: mm).

$S1$	0.2	$S5$	0.3	$la$	4	$l3$	12.7
$S2$	0.2	$w1$	1.6	$lb$	10.9	$ws$	1.2
$S3$	0.5	$w0$	1.6	$lc$	8.8	$c$	8.8
$S4$	0.3	$l0$	2.5	$w3$	1.2		



**Figure 11.** Comparison of  $S$ -parameters between measured and simulated results at port 1 input (a) narrowband, (b) wideband.



**Figure 12.** (a) Measurement and simulation results of output port phase. (b) Measurement and simulation results of output port amplitude imbalance.

displayed separately. The comparison between the measured and simulated results of the phase of the output port is shown in Fig. 12(a). The comparison between the measured and simulated results of the amplitude imbalance of the output port is shown in Fig. 12(b). Through comparison, it can be found that the curve direction of the measured results and simulation results is basically the same. The isolation degree of the coupler is greater than 20 dB, and the 3 dB bandwidth of the filter is 2.35 GHz–2.51 GHz. It can suppress harmonics within the  $8.2f_0$  range by over 18 dB. The phase imbalance within the passband shall not exceed  $9^\circ$ , and the amplitude imbalance shall not exceed 1.2 dB. According to the measured results of  $S$ -parameters, the center frequency of the passband is 2.43 GHz, which is 30 MHz higher than the center frequency of the simulation results. This may be caused by the deviation in the processing of the fine microstrip. The overall insertion loss of the measured passband is slightly higher, with a minimum insertion loss of 3.9 dB, which is 0.6 dB higher than the simulation results. The main reason may be the influence of SMA joint loss and welding discontinuity. According to the comparison between the measured phase results of the output port and the simulation results, it can be seen that the measured phase of the port has moved slightly towards high frequency synchronously

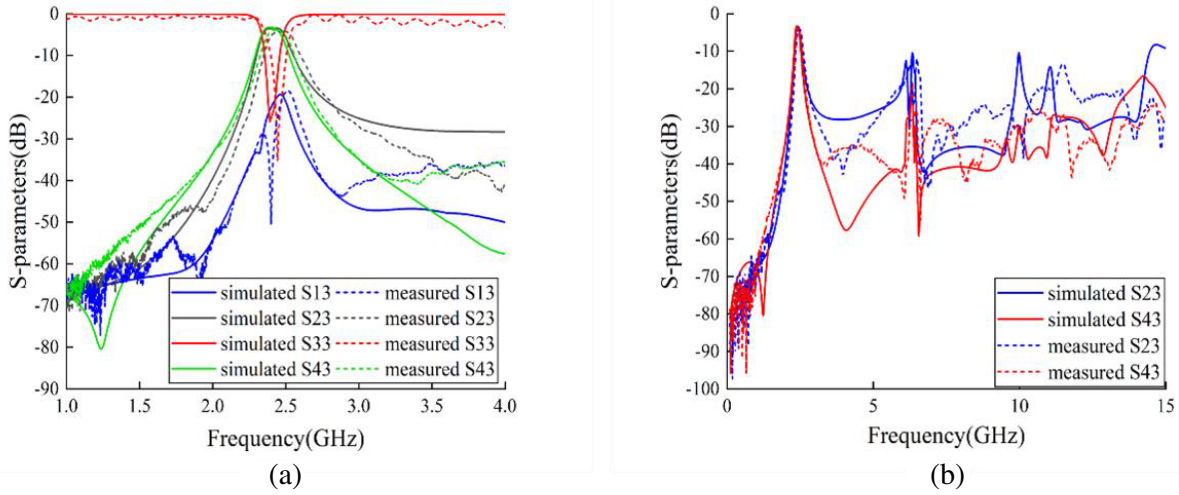


**Figure 13.** Comparison of  $S$ -parameters between measured and simulated results at port 3 input (a) narrowband, (b) wideband.

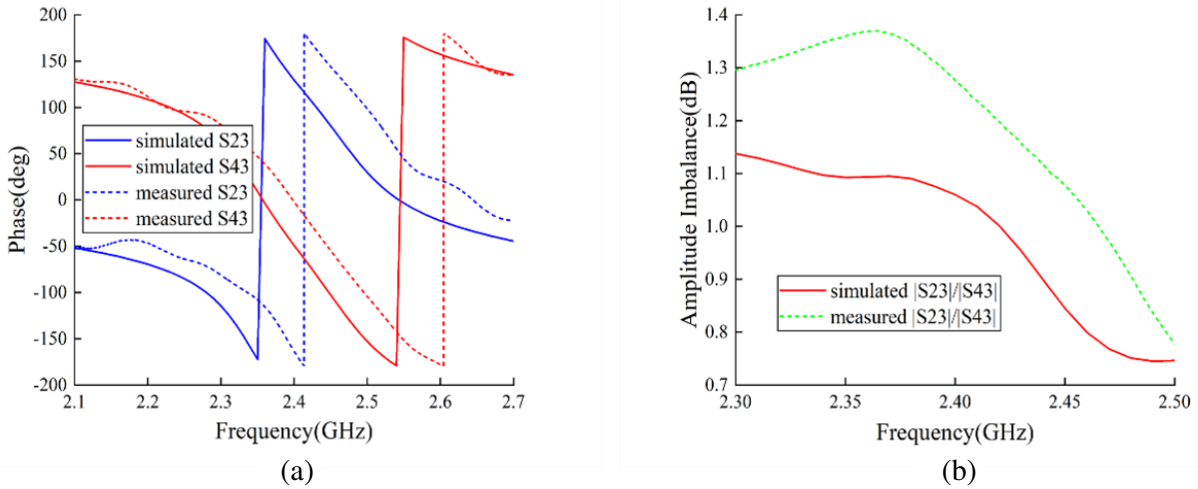


**Figure 14.** (a) Measurement and simulation results of output port phase. (b) Measurement and simulation results of output port amplitude imbalance.

with the center frequency, but the phase difference between the ports has hardly changed.

When port 3 is the input port, the comparison results of the measured and simulated  $S$ -parameters are shown in Fig. 13. For ease of observation, the broadband and narrowband results are displayed separately. The comparison between the measured phase results of the output port and the simulated results is shown in Fig. 14(a). The comparison between the measured amplitude imbalance of the output port and the simulated results is shown in Fig. 14(b). Through comparison, it can be found that the curve directions of the measured and simulated results are basically the same. The isolation degree of the coupler is greater than 20 dB, and the 3 dB bandwidth of the filter is 2.36 GHz–2.51 GHz, which can suppress harmonics within the  $6f_0$  range by more than 10 dB. The phase imbalance within the passband shall not exceed  $10^\circ$ , and the amplitude imbalance shall not exceed 1.4 dB. According to the measured results of the  $S$ -parameter, the center frequency of the passband is 2.435 GHz, which is shifted 35 MHz towards the high frequency compared to the simulation results. The overall insertion loss of the measured passband is slightly higher, with a minimum insertion loss of 3.9 dB, which is 0.6 dB higher than the simulation results. The reason for the error is similar to the previous analysis. According to

the comparison between the measured phase results of the output port and the simulation ones, it can be seen that the measured phase of the port has moved slightly towards high frequency synchronously with the center frequency, but the phase difference between the ports has hardly changed.

From the above analysis, it can be seen that the error of the measured results of the filtering coupler is within a reasonable range and does not affect the overall performance. Therefore, it is acceptable. The test results verify the feasibility of the design method of the filtering coupler. In order to compare the filtering couplers in the reference literature, Table 2 summarizes several similar filtering couplers. Through comparison, it was found that the filtering coupler proposed in this article has excellent performance, compact size, and ultrawide stopband.

**Table 2.** Comparison of various filtering couplers.

Reference	$f_0$ (GHz)	IL (dB)	Stopband width	Size ( $\lambda_g \times \lambda_g$ )
[9]	3.08	0.95	$2.53f_0$ ( $> 20$ dB)	$0.75 \times 0.35$
[11]	2.82	1.3	$5.24f_0$ ( $> 10$ dB)	$0.29 \times 0.26$
[14]	2.4	1.43	$2.2f_0$ ( $> 20$ dB)	$0.185 \times 0.106$
[15]	1.4	1.0	$2.56f_0$ ( $> 10$ dB)	$0.48 \times 0.38$
This Work	2.43	0.9	$8.2f_0$ ( $> 18$ dB)	$0.23 \times 0.33$

## 5. CONCLUSION

In this paper, based on the analysis of external quality factor and coupling coefficient, the collaborative design of filter and coupler is carried out, and a miniaturized and wide stopband high-performance filtering coupler is designed. Firstly, a short-stub loaded uniform-impedance resonator (SSLUIR) was proposed, and its resonant characteristics were analyzed using the  $ABCD$  matrix and admittance parameters. By adjusting the impedance ratio of the stubs and bending them, the size of the SSLUIR was reduced. Then, the resonance performance of SSLUIR during electrical and magnetic coupling was studied. By controlling the electrical length of the short stubs, higher harmonics can be suppressed, and the upper stopband can be widened. Finally, using the analysis method of external quality factor and coupling coefficient, a microstrip 3 dB  $180^\circ$  filtering coupler is designed. The size of the filtering coupler is  $0.23\lambda_g \times 0.33\lambda_g$ , with a harmonic suppression of over 18 dB within the  $8.2f_0$  range. Compared with similar filtering couplers, it has good performance, miniaturization, and wide stopband characteristics.

## ACKNOWLEDGMENT

This work is supported by the Key Natural Science Research Project of Anhui Higher Education Institutions: Research and application on electromagnetic regulation mechanism of artificial magnetic conductor materials 2022AH050070, and the National Nature Science Foundation of China 62101002, U22A2017, U20A20164.

## REFERENCES

1. Shen, G., W. Che, W. Feng, et al., "A miniaturized Ka-band bandpass filter using folded hybrid resonators based on monolithic microwave integrated circuit technology," *IEEE Transactions on Circuits and Systems II: Express Briefs*, Vol. 68, No. 6, 1778–1782, 2021.
2. Seo, J., I. Yoon, J. Jung, et al., "Miniaturized dual-band broadside/endfire antenna-in-package for 5G smartphone," *IEEE Transactions on Antennas and Propagation*, Vol. 69, No. 12, 8100–8114, 2021.
3. Wang, W., Y. Zheng, and Y. Wu, "Miniaturized single-ended-to-balanced arbitrary four-section coupled-line coupler with inherent impedance matching," *IEEE Transactions on Circuits and Systems II: Express Briefs*, Vol. 67, No. 10, 1929–1933, 2020.

4. Ahn, H. R. and M. M. Tentzeris, "Arbitrary power-division branch-line hybrids for high-performance, wideband, and selective harmonic suppressions from  $2f_0$ ," *IEEE Transactions on Microwave Theory and Techniques*, Vol. 67, No. 3, 978–987, 2019.
5. Inaba, T. and H. Hayashi, "3-branch-line coupler with harmonic suppression by using short stubs," *2020 IEEE 9th Global Conference on Consumer Electronics (GCCE)*, 622–623, IEEE, 2020.
6. Liu, I., M. Guan, X. Li, and Z. Wang, "Coupled line forward directional coupler with inherent harmonics suppression at  $2f_0$ ," *2020 Cross Strait Radio Science & Wireless Technology Conference*, 1–3, IEEE, 2020.
7. Lalbakhsh, A., et al., "Design of a compact planar transmission line for miniaturized rat-race coupler with harmonics suppression," *IEEE Access*, Vol. 9, 129207–129217, 2021.
8. Coromina, J., P. Vélez, J. Bonache, and F. Martín, "Branch line couplers with small size and harmonic suppression based on non-periodic step impedance shunt stub (SISS) loaded lines," *IEEE Access*, Vol. 8, 67310–67320, 2020.
9. Dong, G., W. Wang, Y. Wu, et al., "Filtering rat-race couplers with impedance transforming characteristics based on terminated coupled line structures," *IET Microwaves, Antennas & Propagation*, Vol. 14, No. 8, 734–742, 2020.
10. Shao, Q., F. C. Chen, Q. X. Chu, et al., "Novel filtering  $180^\circ$  hybrid coupler and its application to  $2 \times 4$  filtering butler matrix," *IEEE Transactions on Microwave Theory and Techniques*, Vol. 66, No. 7, 3288–3296, 2018.
11. Rezaei, A. and L. Noori, "Microstrip hybrid coupler with a wide stop-band using symmetric structure for wireless applications," *Journal of Microwaves, Optoelectronics and Electromagnetic Applications*, Vol. 17, 23–31, 2018.
12. Zheng, Y., W. Wang, and Y. Wu, "Synthesis of wideband filtering couplers for arbitrary high power-division ratios based on three different types of coupled-line sections," *IEEE Transactions on Circuits and Systems*, Vol. 68, No. 4, 1218–1222, 2021.
13. Wang, X., J. P. Wang, L. Zhu, et al., "Compact stripline dual-band bandpass filters with controllable frequency ratio and high selectivity based on self-coupled resonator," *IEEE Transactions on Microwave Theory and Techniques*, Vol. 68, No. 1, 102–110, 2020.
14. Lin, T.-W., J.-Y. Wu, and J.-T. Kuo, "Compact filtering branch-line coupler with source-load coupling," *2016 IEEE International Workshop on Electromagnetics: Applications and Student Innovation Competition (iWEM)*, 1–3, IEEE, 2016.
15. Zhao, Z., H. Liu, J. Ren, Z. Wang, and S. Fang, "Wideband filtering rat-race coupler with shared triple-mode resonator," *Electronics*, Vol. 12, No. 12, 2701, 2023.